Supporting Information

Few-layered Ti_3C_2 nanosheet/glass fiber composite separator as lithium polysulphide reservoir for high-performance lithium-sulfur battery

Chong Lin[ab], Weikun Zhang[be], Lei Wang[c], Zhenggong Wang[b], Wen Zhao[d], Wenhui Duan[d], Zhigang Zhao[b], Bin Liu[a] and Jian Jin[b*]

[a.] *Key Laboratory of Synthetic and Natural Functional Molecule Chemistry of Ministry of Education, Shanxi Key Laboratory of Physico-Inorganic Chemistry, College of Chemistry & Materials Science, Northwest University, Xi'an 710069, P. R. China.*
[b.] *Suzhou Institute of Nano-Tech and Nano-Bionics, Chinese Academy of Sciences, Suzhou, 215123, P. R. China.*
[c.] *Department of Chemical and Biomolecular Engineering, Johns Hopkins University, Baltimore, Maryland 21218, United States.*
[d.] *Department of Physics, Tsinghua University, Beijing 100084, P. R. China. Address here.*
[e.] *College of Environment and Chemical Engineering, Shanghai University, Shanghai 200444, P. R. China.*

E-mail: jjin2009@sinano.ac.cn

Experimental

1.1 Materials

MAX phase (Ti_3AlC_2, > 97%, Shanghai Yuehuan Material Technology Co., Ltd), LiF (97%, Sigma-Aldrich), HCl (90%, Sinopharm Chemical Reagent Co., Ltd), absolute ethanol (> 99.7%, Sinopharm Chemical Reagent Co., Ltd), commercial sulfur (reagent grade, Sigma-Aldrich), MWCNT (> 95 wt%, OD 30-50 nm, length 0.5-2 μm, Nanjing XF nano, INC), graphene powder (Nanjing XF nano, INC), glass fiber (GF/A, Whatman), NMP (99.5%, Sigma-Aldrich), Al foil (cell grade, Hefei Kejing Material Technology Co., Ltd), PVDF (cell grade, Hefei Kejing Material Technology Co., Ltd), and Super P conductive (Alfa-aser) are used. Milli-Q water is used in the whole work.

1.2 Preparation of bulk Ti_3C_2 and Ti_3C_2 nanosheet

For the synthesis of bulk Ti_3C_2, LiF was dissolved in 6 M HCl, then the MAX phase precursor, Ti_3AlC_2 powder was added slowly into this solution. After that, the mixture was heated at 40°C for 45 h. After etching completely, the resulting dispersates were centrifuged

and washed with water several times to raise the pH. At last, the collected etching Ti_3C_2 were dried at 60°C in a drying oven. To get the Ti_3C_2 nanosheet, dried clay-like multilayer Ti_3C_2 were redispersed in deionized water, followed by ultrasonic for 4 h. After that, the dispersions were centrifuged at 3500 rpm for 60 min and the upper dispersions were collected.

1.3. Preparation of bulk Ti_3C_2, Ti_3C_2 nanosheet, and graphene covered GF separators

The commercial GF separator was firstly prepunched into diameter of 2 cm. Then, bulk Ti_3C_2, Ti_3C_2 nanosheet, and graphene dispersion in water were vacuum-filtrated on the punched GF separator, respectively. Before this, a very little multi-walled carbon nanotubes (MWCNTs) dispersion with negligible weight were filtrated on punched GF separator in order to avoid the mass loss of them caused by the large pore of the GF separator. To balance of the mass of the total weight of the battery, the mass loading of the Ti_3C_2 nanosheet in every separator is 0.6~1 mg. The obtained composite separators were air-oven dried at 60°C for 12 h for further use.

1.4. Preparation of Li_2S_7 and visualized diffusion test

The Li_2S_7 was synthesized by reacting Li_2S and S with the desired ratio in anhydrous THF at room temperature for 2 h in an Ar-filled glovebox. The visualized diffusion test was carried out in an H-type cell. The left chamber was filled with 10 mM Li_2S_7 THF solution and the right chamber was only filled with THF.

1.5. Preparation of Nano-S composite

The raw MWCNTs were treated with concentrated hydrochloric acid for 24 h at room temperature under vigorous stirring. Then, the pretreated MWCNTs were refluxed in the mixture of concentrated nitric acid and sulfuric acid (1:3 by vol.) at 80°C for 10 h and washed by deionized water several times until the pH value changed to 7. After filtration, the modified MWCNTs were dried at 80°C for overnight in a vacuum oven for the subsequent use. 1.4 g commerical bulk S and 0.6 g modified MWCNTs (the weight ratio of S to MWCNTs is 7:3) were grounded in a motar. Then the mixture were transformed to a ZrO_2 jar

(25 mL) filling with 17 ZrO_2 spheres with the diameter of 1 cm and ball-milling for at 300 rpm for 10 cycles (ball-milling for 1 h and pause for half an hour in each cycle). After that, the as-prepared product was collected by deionized water and washed with HF (20 wt%) to clean up the ZrO_2 residual brought from ball-milling. Then the HF treated CNT-S composites were washed by water at least three times and then dried under vacuum overnight for further use. At last, the as-prepared MWCNTs-S composite was heated in tube furnace at 155°C for 24 h under flow argon atmosphere to make sure that S diffused into the MWCNTs.

1.6. Materials Characterization

Scanning electron microscopy (SEM) analysis was performed on a Quanta 400 FEG field-emission scanning electron microscope. Transmission electron microscopy (TEM) analysis was performed on a Tecnai G2 F20 S-Twin field emission transmission electron microscope. Atomic force microscopy (AFM) analysis was performed on a Bruker Dimension Icon atomic force microscope. X-ray diffraction (XRD) was collected on a Bruke D8. Electrochemical measurements were carried out using Land battery analyzers and Autolab PGSTAT302N electrochemical station. Raman analysis was performed on a Horiba LabRAM ARAMIS using a 473 nm laser irradiation.

1.7. Electrochemical Measurements

To prepare the working electrode, the commercial sulfur, super P conductive and PVDF (7:2:1 by weight) were mixed in appropriate volume of NMP by grinding for 4 h to form uniform slurry. After that, the slurry was then coated onto alummium foil using doctor blade method and dried at 60°C in a drying oven to form working electrode. Then, the working electrode was punched into diameter of 14 mm and the mass of which was accurately weighted using a microbalance (Sartarious, 0.001 mg resolution). The average mass loading of the sulfur is ~3 mg. To prepare nano-S electrode, the MWCNTs-S composite, super P conductive and PVDF (7:2:1 by weight) were mixed in an appropriate volume of NMP by grinding for 4 h to form uniform slurry. After that, the slurry was then coated onto aluminum

foil using doctor blade method and dried at 60°C in a drying oven to form working electrode. To test battery performance, 2032 type coin cells were assembled in an argon-filled glove box with H_2O and O_2 content below 0.1 ppm, using the sulfur as working electrode, the Li metal foil as the counter electrodes, and the GF separator with or without bulk Ti_3C_2 or Ti_3C_2 nanosheet, respectively. The electrolyte was freshly prepared from 1 M lithium bis(trifluoromethanesulfony) imide dissolved in the mixture of 1:1 (volume) 1,2-dimethoxyethane and 1,3-dioxolane containing 1 wt% $LiNO_3$. The working electrodes were cycled between 2.8 V and 1.5 V vs Li^+/Li. All the specific capacity values were calculated based on the mass of S in the electrodes. EIS measurements were performed on Autolab PGSTAT302N electrochemical station over the frequency range from 100 KHz to 10 mHz.

1.8. Computational methods

Density functional theory calculations were performed using the Vienna ab initio simulation package (VASP), with the exchange-correlation potential described by PBE version of the generalized gradient approximation. Interactions between ion and electron were described by the projector augmented wave (PAW) approach. The plane-wave cutoff was set to 400 eV, and the total energy was converged to 10^{-4} eV. The Ti_3C_2, $Ti_3C_2F_2$, and $Ti_3C_2(OH)_2$ systems were modeled by 4 × 4 supercells with vacuums ~20 Å in the vertical direction. Brillouin zone was sampled by a 3×3×1 Γ-centered k-point grid for relaxation. Atomic positions and lattice parameters were fully relaxed until the residual Hellmann-Feynman force on each atom was less than 0.05 eV/ Å. The binding energy (E_{bind}) of a lithium polysulfide cluster on a Ti_3C_2 nanosheet is defined as $E_{bind} = E(Ti_3C_2) + E(Li_2S_x) - E(Ti_3C_2\text{-}Li_2S_x)$ (x = 1, 4, 6 and 8), where $E(Ti_3C_2)$, $E(Li_2S_x)$, and $E(Ti_3C_2\text{-}Li_2S_x)$ are the total energies of Ti_3C_2 host, Li_2S_x clusters and $Ti_3C_2\text{-}Li_2S_x$ composite, respectively. A larger positive value means higher stability.

2. Supplemental Figures:

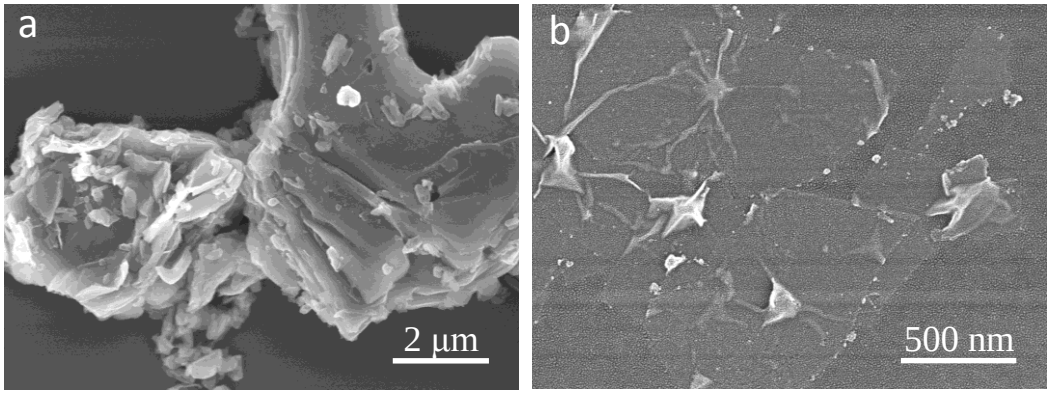

Figure S1. SEM images of bulk Ti_3C_2 (a) and delaminated Ti_3C_2 nanosheet (b).

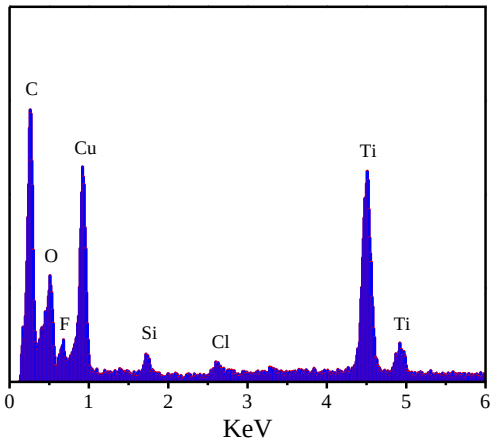

Figure S2. EDAX of Ti_3C_2 nanosheet.

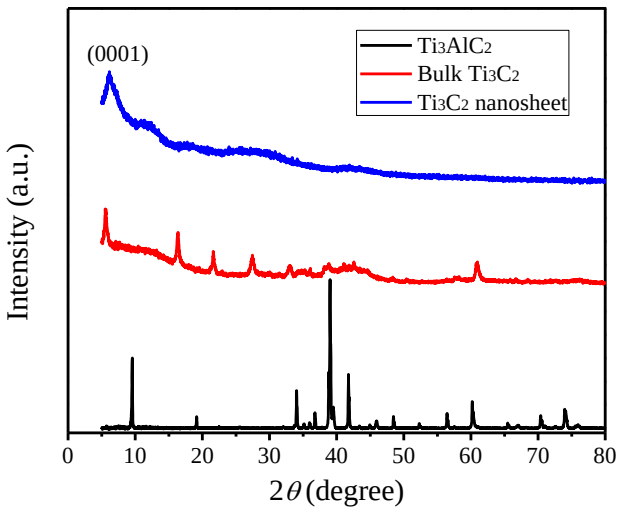

Figure S3. XRD of Ti_3AlC_2, bulk Ti_3C_2 and Ti_3C_2 nanosheet.

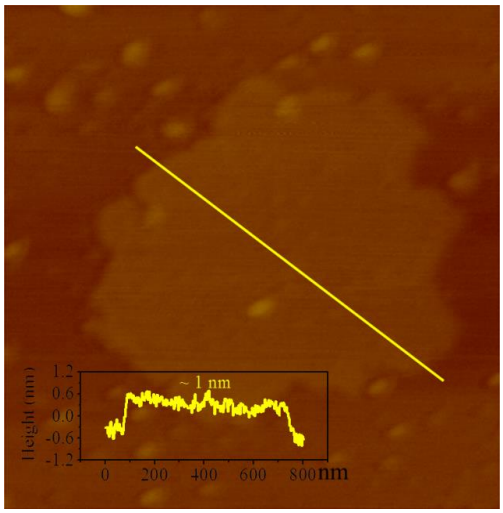

Figure S4. AFM image of single layer Ti_3C_2 nanosheet with thickness of ~ 1 nm.

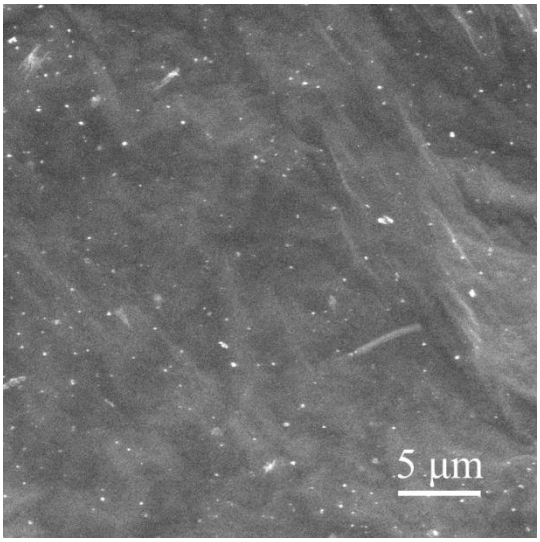

Figure S5. SEM image of graphene covered GF separator.

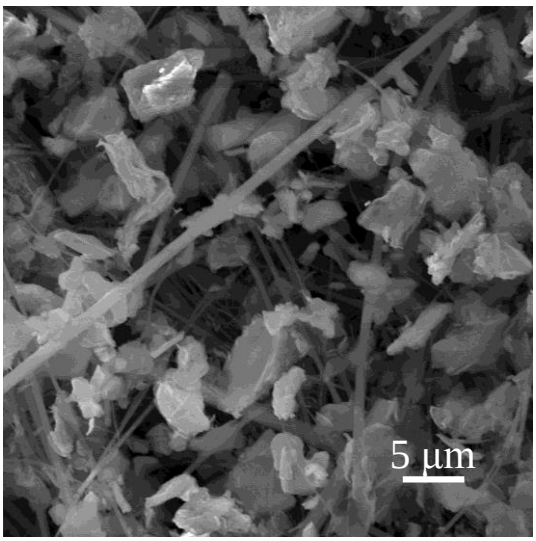

Figure S6. SEM image of bulk Ti_3C_2 covered GF separator.

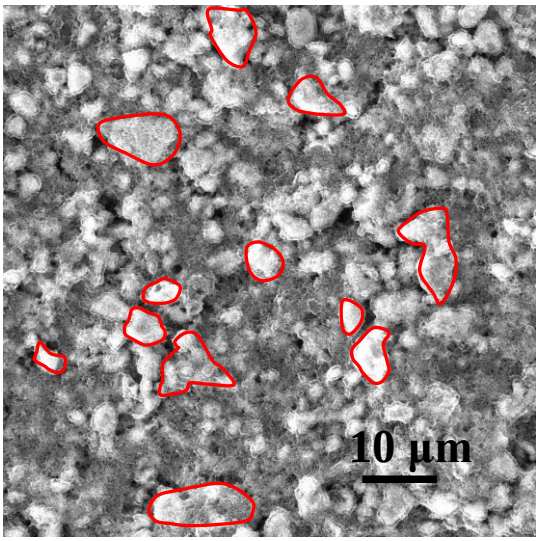

Figure S7. SEM image of the sulfur cathode. The size of bulk sulfur without any treatment is in the range of 2-10 µm.

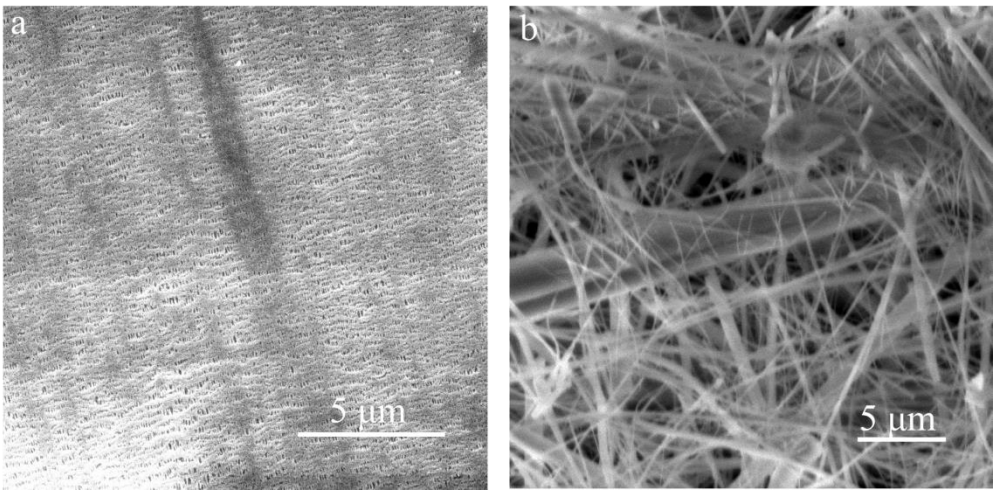

Figure S8. SEM images of (a) polymeric separator (Celgard 2350) and (b) GF separator.

Table S1. Comparison of discharge capacities using GF separator and polymeric separator considering the weight of S cathode and the total weight of the whole cell, respectively.

	Weight (mg)	**Discharge capacity (mAh/g)**			**Discharge capacity(mAh/g_{total})**
		1^{st} (0.1A/g)	2^{nd} (0.5A/g)	100^{th} (0.5A/g)	100^{th} (0.5A/g)
GF separator	15.5	1067	490	366	40
Polymeric separator	3.9	956	148	49	14

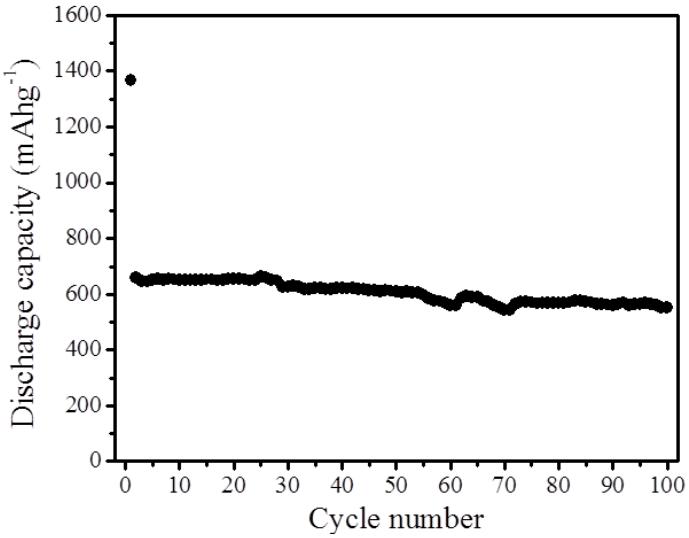

Figure S9. Cycling performance at the current density of 0.5 A/g with bulk Ti_3C_2 covered GF composite separator.

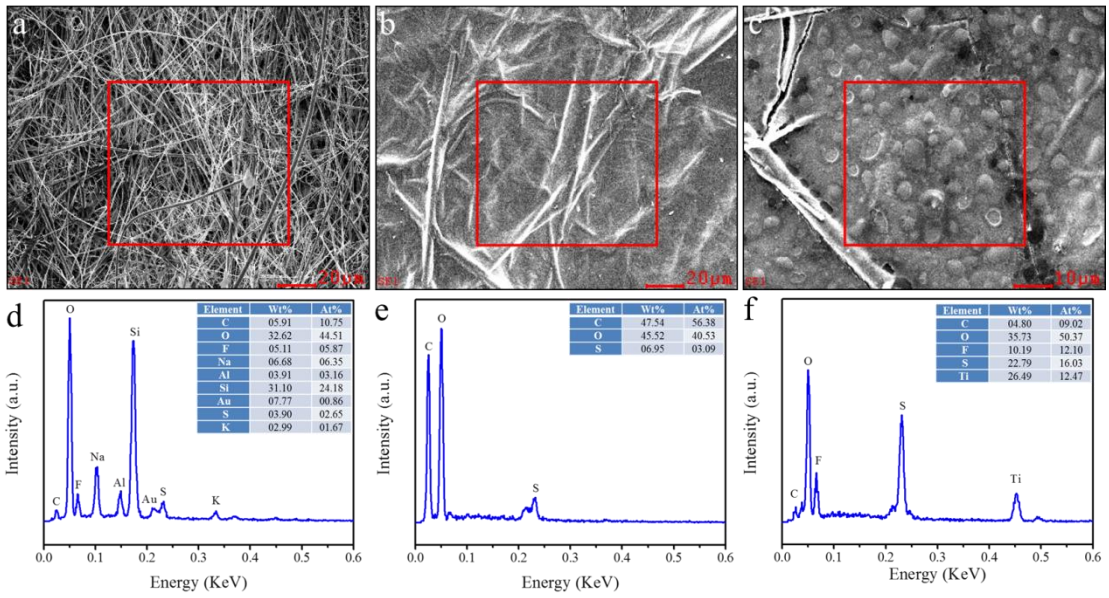

Figure S10. (a-c) SEM images of GF separator, graphene covered GF composite separator, and Ti_3C_2 nanosheet covered GF composite separator at the end of 100^{th} charge to 2.8 V. (d-f) are their corresponding EDS spectra. The inset tables are their corresponding elemental contents percentage. Obviously, the sulfur content percentage in the Ti_3C_2 nanosheet covered GF separator is extremely higher than the other two separators, indicating the function of Ti_3C_2 nanosheet at alleviating the dissolution of LiPSs in the electrolyte and improving their redeposition process upon discharge/charge, thereby improving the performance of Li-S battery.

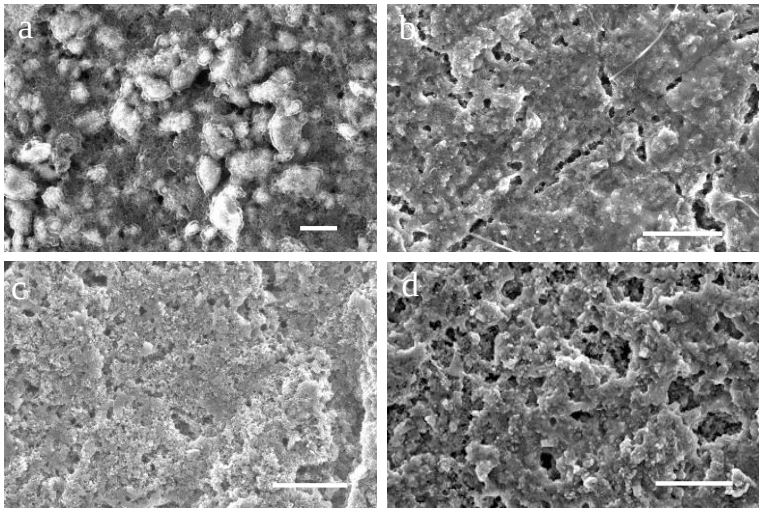

Figure S11. (a) SEM image of S cathode before cycle. SEM images of S cathodes at the end of 100th charge to 2.8 V with the use of GF (b), graphene/GF composite (c), and Ti_3C_2 nanosheet/GF composite (d) separators. Scale bar: 10 μm. The bright and white sulfur particles in the size of 2-10 μm could be clearly observed in Figure S11a. After cycling, the morphologies of sulfur cathodes hange a lot. The large sulfur particles could not be observed in the cycled cathodes. The pockmarks made by sulfur consumption are left on the cathode. In general, a high battery performance indicates a high usage of sulfur which leads to a large morphological change of sulfur cathodes. In our work, the lost sulfur could be effectively captured by Ti_3C_2 nanosheet covered GF composite separator and thus a better Li-S performance is achieved.

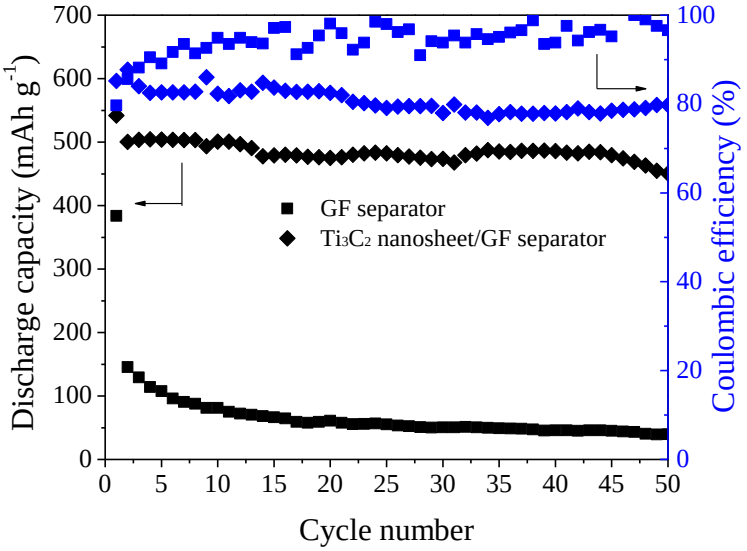

Figure S12. The bulk sulfur cathode cycled at the current density of 0.5 A/g by using $LiNO_3$-free electrolyte with GF separator and Ti_3C_2 nanosheet/GF separator, respectively. It shows that without Ti_3C_2 nanosheets coating, the sulfur cathode delivers a very cycle stability and poor Coulombic efficiency. The Ti_3C_2 nanosheet/ GF composite separator exhibits a much improved cell performance, suggesting a low LiPSs shuttle effect.

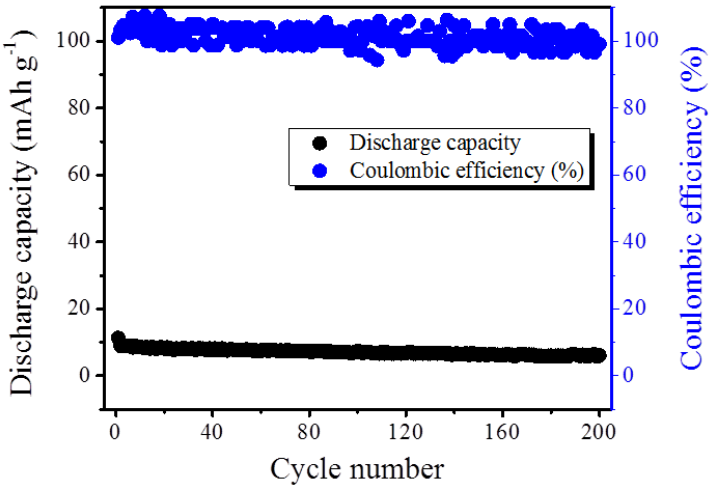

Figure S13. Ti_3C_2 nanosheet covered GF composite separator without sulfur cathode cycled at the current density of 0.5 A/g. The capacity contributed by Ti_3C_2 nanosheet is negligible.

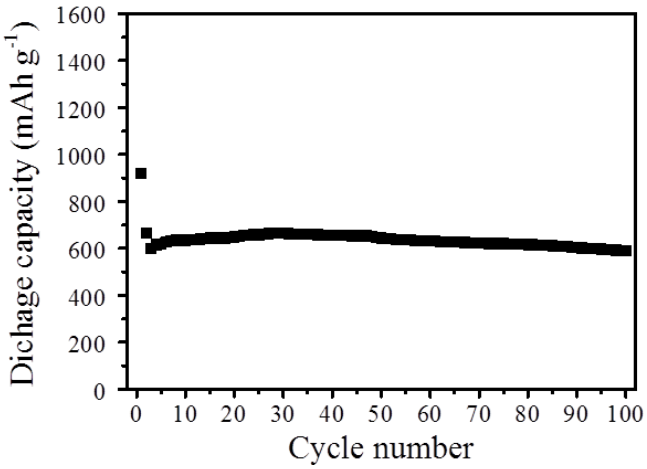

Figure S14. Cycling performance of Ti_3C_2 nanosheet covered GF composite separator at the current density of 1.5 A/g. The sulfur cathode delivers a discharge capacity of 666 mAh/g and the discharge capacity is 591 mAh/g over 100 cycles.

Table S2. Electrochemical performance of Li–S cells based on different composite separators.

Separator	S loading (%)	Rate	Initial capacity (mAh/g)	Cycle capacity (mAh/g/cycle)	Ref.
Al_2O_3/PP	60	0.2 C	898	432/50th	S1
Nafion	—	0.2 C	1400	650/100th	S2
Li-Nafion@Celgard	45	0.5 C	~700	—	S3
graphene/polypropylene/Al_2O_3 (GPA)	75	0.1 C	~1068	~804/100th	S4
MCNT/Celgard	70	0.5C	~1000	~800/100th	S5
MCNT@PEG/ Celgard	60	0.5 C	~1200	~490/500th	S6
Al_2O_3–Super P/PP	70	0.2 C	700	300/50th	S7
Super P/PP	70	0.1 C	836	~600/100th	S7
GF/PP	50	0.5 C	1010	735/100th	S8
Ti_3C_2/GF	70	0.5 A/g	820	721/100th	This work

References

S1. Z. Zhang, Y. Lai, Z. Zhang, K. Zhang and J. Li, *Electrochim. Acta*., 2014, **129**, 55-61.
S2. X. Yu, J. Joseph and A. Manthiram, *J. Mater. Chem. A.*, 2015, **3**, 15683-15691.
S3. I. Bauer, S. Thieme, J. Brückner, H. Althues and S. Kaskel, *J. Power Sources*., 2014, **251**, 417-422.
S4. R. Song, R. Fang, L. Wen, Y. Shi, S. Wang and F. Li, *J. Power Sources*., 2016, **301**, 179-186.
S5. S.-H. Chung and A. Manthiram, *J. Phys. Chem. Lett.*, 2014, **5**, 1978-1983.
S6. G. Wang, Y. Lai, Z. Zhang, J. Li and Z. Zhang, *J. Mater. Chem. A.*, 2015, **3**, 7139-7144.
S7. H. Yao, K. Yan, W. Li, G. Zheng, D. Kong, Z. W. Seh, V. K. Narasimhan, Z. Liang and Y. Cui, *Energy Environ. Sci.*, 2014, **7**, 3381-3390.
S8. L. Wang, J. Liu, S. Haller, Y. Wang and Y. Xia, *Chem. Commun.*, 2015, **51**, 6996-6999.

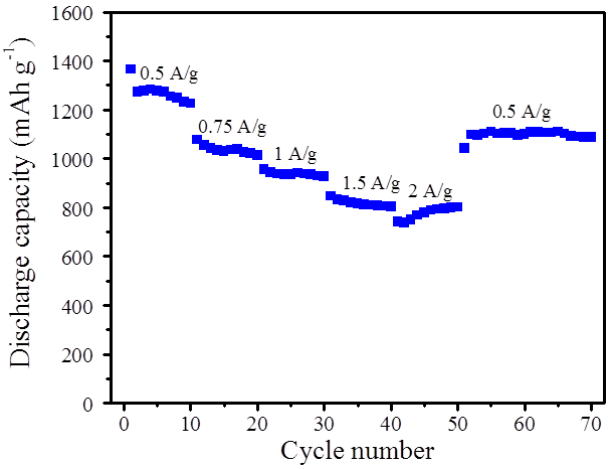

Figure S15. Rate performance of nano-S cathode cycled with Ti_3C_2 nanosheet covered GF composite separator at different current densities. It shows reversible charge capacities of 1366, 1166, 1014, 928 and 802 mAh/g at the current density of 0.5, 0.75, 1, 1.5, and 2 A/g (each for 10 cycles), respectively.

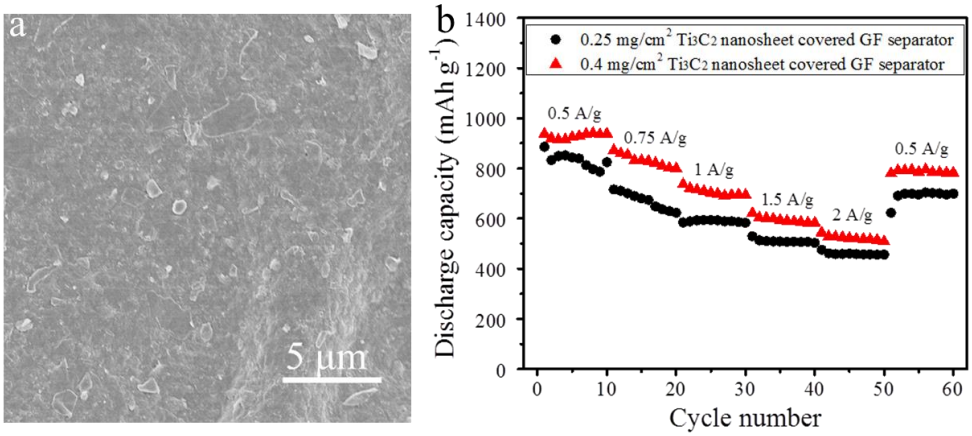

Figure S16. (a) SEM image of 0.4 mg/cm^2 Ti_3C_2 nanosheet covered GF composite separator. The glass fibers are completely overlapped by these flakes. (b) Rate performance of 0.25 mg/cm^2 and 0.4 mg/cm^2 Ti_3C_2 nanosheet covered GF composite separators cycled at different current densities. They show a reversible charge capacity of 886, 716, 589, 530 and 476 mAh/g and 937, 872, 736, 621 and 545 mAh/g at the current density of 0.5, 0.75, 1, 1.5, and 2 A/g (each for 10 cycles), respectively. To evaluate the effect of pore sizes of the separators on cell performance, we calculated the porosities of the four different separators by weighing the mass of each electrolyte-wetting separators. The obtained porosities are 43.5%, 90.1%, 82.7% and 87.8% and the electrolyte up-take rates are 1.7, 10.1, 8.2 and 7.5 corresponding to polymeric, GF, Graphene and Ti_3C_2 nanosheet/GF separators, respectively. It shows that graphene/GF separator and Ti_3C_2 nanosheet/GF separator possess higher porosity and electrolyte up-take rate than polymeric and GF separators. The results of cell performance indicate that the high porosity and high electrolyte up-take rate is good for achieving high capacity and cycle stability.

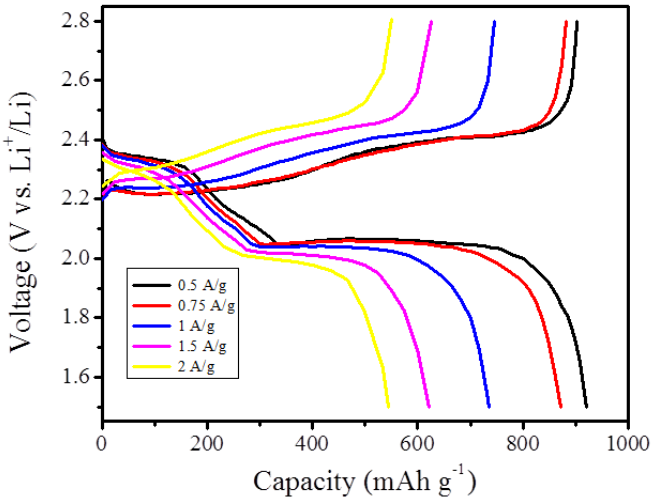

Figure S17. Voltage profiles of S cathode by use of Ti_3C_2 nanosheet covered GF composite separator cycled at various current densities from 0.5 to 2 A/g. Figure S15 shows the typical discharge/charge profiles of the cell at different current densities of 0.5, 0.75, 1, 1.5, and 2 A/g in the potential range of 2.8−1.5 V at room temperature in which the mass loading of Ti_3C_2 nanosheet reach to 0.4 mg/cm^2 (~1 mg) whose performance is further enhanced compared with low mass loading of Ti_3C_2 nanosheet. But the mass of whole batteries will be too large to improve its specific capacity based on the mass of whole cells. The discharge

profiles of all five current densities are characterized by a two-plateau behavior of typical S cathode.

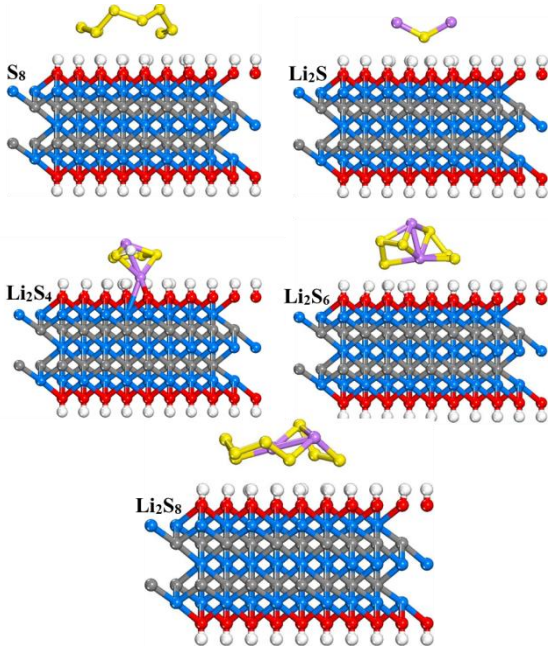

Figure S18. The ab initio calculated structures of S_8, Li_2S, Li_2S_4, Li_2S_6 and Li_2S_8 adsorbed on $Ti_3C_2(OH)_2$. Blue, grey, yellow, purple, red and white balls represent Ti, C, S, Li, O and H, respectively.

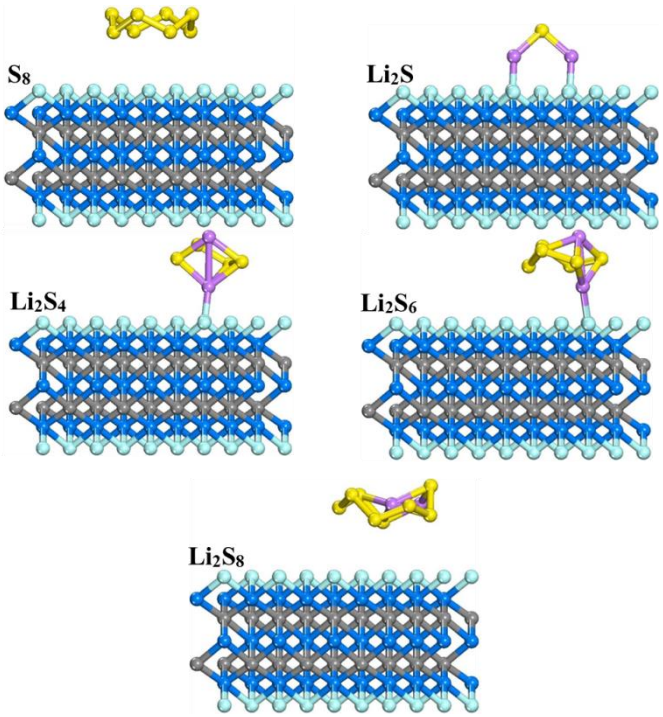

Figure S19. The ab initio calculated structures of S_8, Li_2S, Li_2S_4, Li_2S_6 and Li_2S_8 adsorbed on $Ti_3C_2F_2$. Blue, grey, yellow, purple and cyan balls represent Ti, C, S, Li and F, respectively.

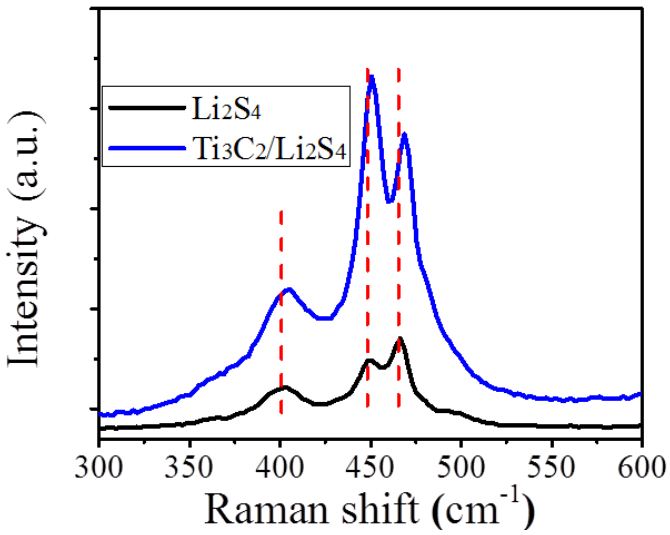

Figure S20. Raman spectra of representative Li_2S_4 (bottom, black) and Ti_3C_2/Li_2S_4 (top, red) to highlight the S−Ti interaction. Three peaks at 400, 448 and 465 cm^{-1} in Li_2S_4 shift to 405, 451 and 469 cm^{-1} when Ti_3C_2 is added to the system. The peak shifts show that the environment around the surface S atoms is changed in the presence of Ti_3C_2. So, it indicates that the Ti_3C_2 nanosheet modified GF composite separator not only suppresses the detachment of S and LiPSs, but also reduces the resistance of the cathode.

Table S3. Comparison of sheet resistances of different separators.

Separator	Polymeric	GF	Graphene/GF	Ti_3C_2/GF
sheet resistance (Ω/□)	8949	41.4	8.6	4.6